The phase diagram of halogens on Pt(110): structure of the (4 × 1)-Br/Pt(110) phase



2009 J. Phys.: Condens. Matter 21 134003

(http://iopscience.iop.org/0953-8984/21/13/134003)

J. Phys.: Condens. Matter **21** (2009) 134003 (7pp) doi:10.1088/0953-8984/21/13/134003

# The phase diagram of halogens on Pt(110): structure of the (4 × 1)-Br/Pt(110) phase

**C Deisl[1], E Dona[1], S Penner[1], M Gabl[1], E Bertel[1], R Zucca[2] and J Redinger[2]**

[1] Institute of Physical Chemistry, University of Innsbruck, Austria
[2] Institute of General Physics and Center for Computational Materials Science, Vienna University of Technology, Austria

Received 13 October 2008, in final form 24 October 2008
Published 12 March 2009
Online at stacks.iop.org/JPhysCM/21/134003

**Abstract**
When adsorbed on the strongly anisotropic Pt(110) surface Br forms a sequence of $(n \times 1)$ structures. In the present study we investigate the $(4 \times 1)$ structure by scanning tunneling microscopy, quantitative low-energy electron diffraction and density-functional calculations. We show that the optimal structural model contains essentially the same adsorption sites as the $(3 \times 1)$ structure, but with a different preference. The positions of the substrate atom are consistent with a frozen surface phonon of fourfold periodicity, suggesting that the phase diagram can be understood on the basis of a tunable charge density wave (Swamy *et al* 2001 *Phys. Rev.* B **86** 1299). The structure could also be explained by assuming short-range interactions only, but evidence is presented that adsorbate–adsorbate interactions mediated by quasi-one-dimensional surface resonances play a major role in both cases.

## 1. Introduction

Pt(110) is a peculiar surface in that the density of states (DOS) at the Fermi level is determined to a large extent by surface resonances. This is the case because the surface resonance band structure features saddle points very close to $E_F$, and in two-dimensional systems saddle points are associated with a divergent DOS. Angle-resolved photoemission experiments show that the curvature in the saddle points is strongly anisotropic and that the bandwidth along the close-packed (cp) rows amounts to ∼1.8 eV, while the perpendicular bandwidth is only 180 meV [2]. The latter is already comparable to thermal energies at moderately elevated temperatures and leads to an anomalous temperature dependence of quasi-particle peaks at $E_F$ in photoemission [2, 3]. The peculiar electronic structure of the surface is accompanied by the occurrence of unusual adsorbate phases. H for instance, which prefers highly coordinated bonding sites on virtually all transition metals where it has been investigated, occupies short-bridge sites on top of the cp rows of the Pt(110) surface [4]. At higher coverages and low temperatures H induces a $(1 \times 4)$ pairing-row–missing-row reconstruction [5].

The phase diagram of halogens on Pt(110) is similarly extraordinary. At half a monolayer [ML; 1 ML is defined by the atom density of the $(1 \times 1)$-Pt(110) surface] coverage Br atoms adsorb on every second short-bridge site on the cp rows and form a $c(2 \times 2)$ structure on the $(1 \times 1)$-Pt(110) surface, with the missing-row reconstruction being lifted [6]. The $c(2 \times 2)$ phase corresponds to a quasi-hexagonal packing, indicating that repulsive interactions are significant. Strangely, as $T$ is lowered to 50 K, long-range order is lost and, in addition to the $c(2 \times 2)$ phase, domains of $(2 \times 1)$ and $(3 \times 2)$ structures appear [7]. In the $(2 \times 1)$ structure Br still occupies every second short-bridge site, but now the Br atoms line up into chains perpendicular to the cp rows. In the $(3 \times 2)$ structure Br atoms occupy every third short-bridge site along the cp rows and additionally every second long-bridge site in between, yielding a $(3 \times 2)$ unit cell as illustrated in figure 1. Such a 'reverse' order–disorder transition can only be understood in terms of a substrate-driven phase transition. A possible explanation is an incipient Peierls transition in the substrate surface, which in view of the strong anisotropy is not entirely unexpected [1, 8]. In quasi-one-dimensional (1D) systems one expects extended Fermi surface nesting, and consequently the formation of charge density waves (CDWs) [9]. Alternatively, the presence of saddle points at $E_F$ could also promote the formation of a Peierls phase [10].

Increasing the Br coverage leads to a succession of $(n \times 1)$ structures, as shown in figure 2. This is usually the signature of a sequence of compression structures, but in the present case the unconventional adsorbate phases and phase transitions suggest the possibility of a more complex behavior. Indeed,

 

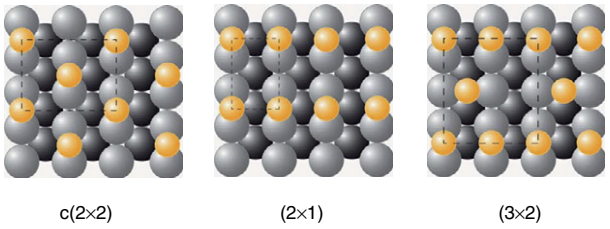


**Figure 1.** Various Br/Pt(110) overstructures observed simultaneously at $T = 50$ K for a coverage of 0.5 ML. At 300 K only the c(2 × 2) structure is stable.

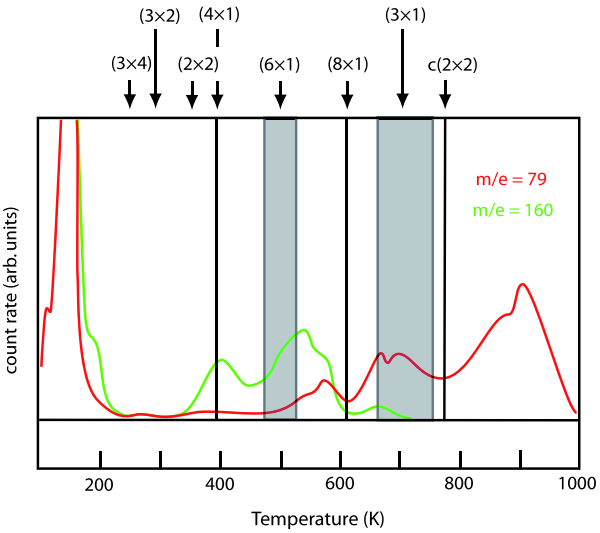


**Figure 2.** Succession of ordered structures of Br on Pt(110) as a function of desorption temperature, starting from a multilayer of Br deposited at 100 K. Note the series of ($n \times 1$) structures occurring between 400 and 780 K. This corresponds to a coverage ranging from 0.75 to 0.5 ML. Under these preparation conditions the missing-row reconstruction is lifted, hence the ($n \times 1$) structures are formed on the (1 × 1)-Pt(110) surface.

at a coverage of 0.67 ML a (3 × 1) structure is formed [11], which can be thought of as being obtained from the (3 × 2) structure by filling the second long-bridge site in the (3 × 2) unit cell, although the (3 × 2) pattern is not observed at room temperature and appears only as a minority species at 50 K. At $\Theta = 0.75$ ML, a (4 × 1) structure appears. In the following this structure is analyzed in detail in order to complement the Br/Pt(110) phase diagram and eventually to obtain a better understanding of the relevant interactions in this unusual adsorbate system. The results demonstrate the importance of the electronic properties of the substrate in dictating the adsorbate geometries. The quasi-1D character of the system manifests itself in the particular succession of adsorbate structures.

## 2. Experimental and computational details

The experiments were carried out in a UHV system with a base pressure of $8 \times 10^{-11}$ mbar. The Pt(110) crystal was cut with a precision of ±0.3° and cleaned according to procedures described in detail previously [12]. Bromine was dosed by

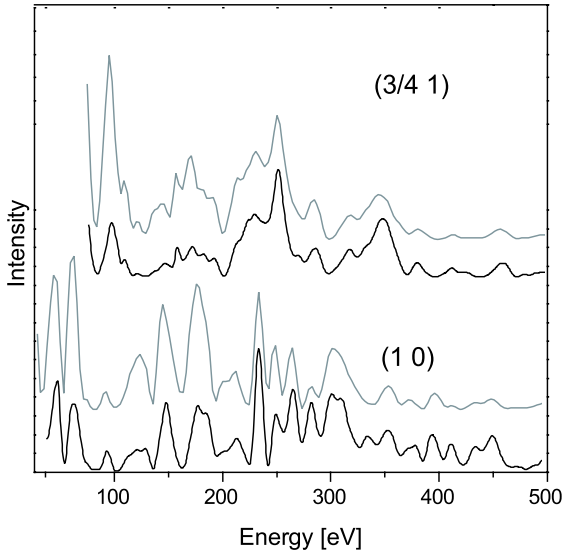


**Figure 3.** LEED intensity versus energy for a fractional and an integer order spot, respectively. Black, measured IV-LEED curve; gray, calculated IV-LEED curve as obtained for the structural model shown in figure 5.

means of a solid state electrolysis cell. The (4×1) structure was obtained by first preparing a c(2×2) structure [6], subsequently dosing additional Br (>0.25 ML) and annealing the system to $T = 400$ K. The scanning tunneling microscope (STM) images were recorded at room temperature.

For the low-energy electron diffraction (LEED) structure determination the LEED pattern was recorded by a high-sensitivity CCD camera while the primary energy of the electrons was varied from 40 to 500 eV. The spot intensities were later evaluated as described in [6]. Typical $I$–$V$ curves are displayed in figure 3. The accumulated data base width was 2352 eV for integral order and 3618 eV for fractional order spots. Seven integral order and eleven fractional order spots where measured. Analysis of the IV-LEED data was carried out using the TENSERLEED program package [13]. The same energy-dependent inner potential was used as in the determination of the (3 × 1) structure [11]. Optimization of each structural model was started with an unrelaxed Pt substrate. The $z$-positions of atoms in the top five layers where independently varied in 0.01 Å steps, as was the case for the $x$, $y$ positions apart from the constraints imposed by the unit cell symmetry. Isotropic vibrational amplitudes for the top three layers were used as fit parameters.

First-principles density functional theory (DFT) calculations were performed by means of the Vienna *ab initio* Simulation Package (VASP) [14], using the projector augmented wave [15] scheme as implemented by Kresse and Joubert [16]. As in our previous papers [6, 11] two DFT potential approximations have been used: the generalized gradient approximation (GGA) according to Perdew and Wang (PW91) [17] and the local density approximation (LDA) as given by Perdew–Zunger (Ceperly–Alder) [18]. A repeated slab with a thickness of 9 or 11 Pt layers with a single Br ad-layer on one side was used, separated by 12 or 14 Å thick vacuum layers. A 3×12×1

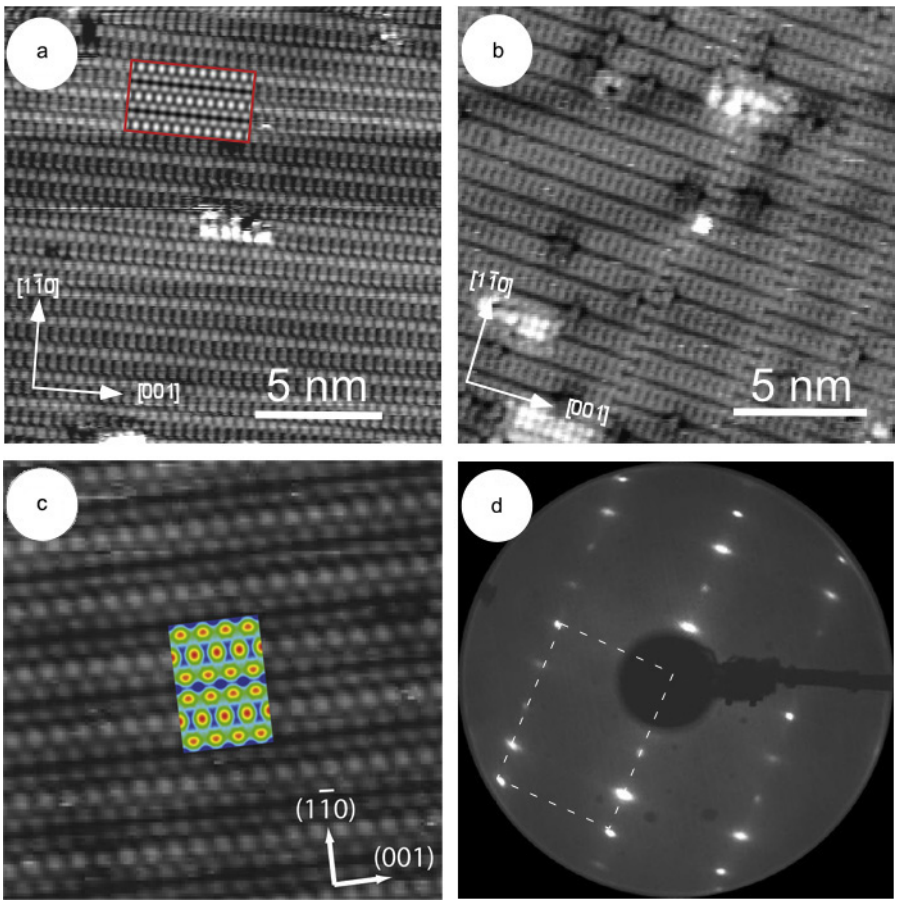


**Figure 4.** (a) Large-scale STM scan of a Br induced (4 × 1) structure on Pt(110) (308 mV; 0.1 nA). The inset (red frame) shows a calculated STM image as described in the text; (b) large-scale STM image recorded at lower tunneling resistance showing inverted contrast (−40 mV; 0.57 nA); (c) (4 × 1) preparation at a bias of 450 mV. The colored inset again shows a calculated STM image, where blue relates to low and red to high local density of states; (d) LEED image of the Br induced (4 × 1) structure on Pt(110). The white rectangle marks the (1 × 1) unit cell.

or 4 × 12 × 1 Monkhorst–Pack type $k$-point mesh and an energy cutoff of 230 eV proved to be sufficiently accurate for the present purposes. The latter was validated by performing the nine-layer calculations with a 400 eV cutoff. All layers were relaxed until all forces were smaller than 0.01 eV Å$^{-1}$, except for three layers on the far side of the nine-layer Pt substrate which had been frozen to the geometry of a clean relaxed p(1 × 1) Pt(110) surface. This setup allowed a very accurate determination of the relaxation in the ad-layer substrate complex and also for layers deeper in the bulk, which turned out to be quite substantial.

## 3. Results

Typical STM images of the (4 × 1)-Br/Pt(110) surface together with the corresponding LEED pattern and a simulated STM image on the basis of the Tersoff–Hamann model [19] are shown in figure 4. The experimental STM image shown in figure 4(a) exhibits a striking agreement with the calculated image displayed as an inset in figures 4(a) and (c). Figure 4(b) shows an STM image, as it was also occasionally measured on the (4 × 1) structure. Dark lines extending along the [001] direction with a periodicity of 11 Å (≈4 × 2.77 Å) in [1$\bar{1}$0] direction are separated by bright double spots oriented in the [1$\bar{1}$0] direction with spacing of 3.92 Å in the [001] direction. The long-range order is perturbed by characteristic anti-phase domain boundaries in the [1$\bar{1}$0] direction. The displacement vector between neighboring domains amounts to two nearest neighbor distances (5.54 Å) in the [1$\bar{1}$0] direction. Figure 4(c) shows part of the image after inversion. Obviously this is the same structure as shown in figure 4(a). The contrast inversion appears to be related to the low tunneling resistance, which, for instance, could lead to the picking up of a Br atom by the tip. It is difficult to determine the precise coverage from the temperature programmed desorption (TPD) spectrum, because desorption from Br layers with $\Theta_{Br} > 0.5$ ML occurs partially as molecular $Br_2$. However, from the excess exposures needed to prepare the (4 × 1) starting from the c(2 × 2) structure we estimate a total coverage of less than 1 ML. It is then natural to assume three Br atoms per unit cell, which results in an ideal coverage of $\Theta_{Br} = 0.75$ ML.

Further structural analysis was carried out by means of the IV-LEED data. A typical LEED image is shown in figure 4(d). Guided by the DFT results and the previously solved (3 × 1) structure [11], we started with structural models exhibiting two Br atoms in short-bridge sites and one Br atom in the

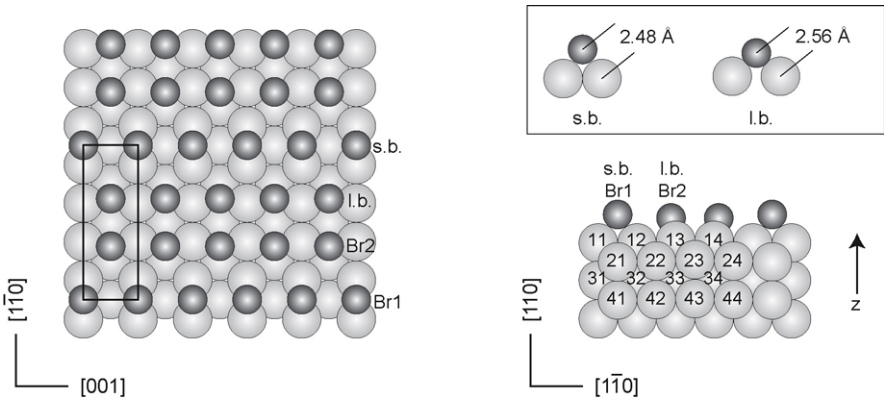


**Figure 5.** Ball model of the (4 × 1)-Br/Pt(110) structure. The unit cell is marked by the black rectangle. Numbers on the atoms refer to the parameter values given in table 1.

**Table 1.** Parameter values for the (4 × 1)-Br/Pt(110) structural model. Values are given in Å. Error limits are ±0.02 Å for the layer-to-layer distances $\Delta d_{ij}$, ±0.03 Å for the $z$-positions $z_{ik}$ of the atoms measured relative to the layer position and ±0.065 Å for the lateral positions $x_{ik}$. $d_{\mathrm{Br}}$ is the Br layer distance. Figure 5 should be consulted for the meaning of the indices. The bulk interlayer distances are 1.382 Å for LDA, 1.409 Å for GGA, and 1.386 Å for LEED.

| | $d_{\mathrm{Br}}$ | $\Delta d_{12}$ | $\Delta d_{23}$ | $\Delta d_{34}$ | $\Delta d_{45}$ | $z_{\mathrm{Br1}}$ | $z_{\mathrm{Br2}}$ | $x_{\mathrm{Br2}}$ |
|---|---|---|---|---|---|---|---|---|
| LEED | 1.79 | −0.02 | 0.03 | 0.01 | 0.00 | 0.17 | −0.08 | −0.38 |
| LDA-11L | 1.77 | −0.03 | 0.01 | 0.02 | −0.01 | 0.16 | −0.08 | −0.34 |
| GGA-11L | 1.83 | −0.02 | 0.01 | 0.02 | 0.00 | 0.15 | −0.07 | −0.35 |
| GGA-9L | 1.83 | −0.02 | 0.01 | 0.02 | 0.00 | 0.14 | −0.07 | −0.36 |
| | $z_{11}$ | $z_{12}$ | $z_{13}$ | $z_{14}$ | $x_{11}$ | $x_{12}$ | $x_{13}$ | $x_{14}$ |
| LEED | −0.09 | −0.09 | 0.09 | 0.09 | 0.09 | −0.09 | −0.10 | 0.10 |
| LDA-11L | −0.12 | −0.12 | 0.12 | 0.12 | 0.04 | −0.04 | −0.08 | 0.08 |
| GGA-11L | −0.13 | −0.13 | 0.13 | 0.13 | 0.05 | −0.05 | −0.12 | 0.12 |
| GGA-9L | −0.14 | −0.14 | 0.14 | 0.14 | 0.04 | −0.04 | −0.10 | 0.10 |
| | $z_{21}$ | $z_{22}$ | $z_{23}$ | $z_{24}$ | $x_{21}$ | $x_{22}$ | $x_{23}$ | $x_{24}$ |
| LEED | −0.07 | −0.01 | 0.10 | −0.01 | — | 0.06 | — | −0.06 |
| LDA-11L | −0.10 | −0.01 | 0.12 | −0.01 | — | 0.03 | — | −0.03 |
| GGA-11L | −0.12 | 0.00 | 0.13 | 0.00 | — | 0.04 | — | −0.04 |
| GGA-9L | −0.12 | −0.01 | 0.14 | −0.01 | — | 0.04 | — | −0.04 |
| | $z_{31}$ | $z_{32}$ | $z_{33}$ | $z_{34}$ | $z_{41}$ | $z_{42}$ | $z_{43}$ | $z_{44}$ |
| LEED | −0.02 | −0.02 | 0.02 | 0.02 | −0.03 | −0.01 | 0.04 | −0.01 |
| LDA-11L | −0.04 | −0.04 | 0.04 | 0.04 | −0.05 | 0.00 | 0.04 | 0.00 |
| GGA-11L | −0.04 | −0.04 | 0.04 | 0.04 | −0.06 | 0.00 | 0.05 | 0.00 |
| GGA-9L | −0.04 | −0.04 | 0.04 | 0.04 | −0.05 | 0.00 | 0.05 | 0.00 |

long-bridge position, or vice versa. Although the short-bridge site is the one yielding the highest binding energy per Br atom, we could not arrive at a reasonable Pendry $R$-factor with the former assumption. $R_{\mathrm{P}}$ remained above 0.55 for this input model. In contrast a TENSERLEED calculation using a starting model with two Br atoms in long-bridge sites converged to $R_{\mathrm{P}} = 0.25$ (0.23 for integral and 0.26 for fractional order spots). This is comparable to our previous structural analyses of the clean missing-row reconstructed Pt(110) surface ($R_{\mathrm{P}} = 0.22$), the c(2×2) structure ($R_{\mathrm{P}} = 0.23$) and the (3 × 1) structure ($R_{\mathrm{P}} = 0.22$). The (4 × 1)-Br/Pt(110) structure determined in this way is displayed in figure 5 and the structural parameters are given in table 1. Br atoms sit on every fourth short-bridge site along the close-packed Pt atom rows and on the two neighboring long-bridge sites in between. Apparently there is a considerable repulsion between the Br atoms in the neighboring long-bridge sites, resulting in a large horizontal displacement (0.38 Å) of the Br atoms out of the ideal long-bridge position.

As already observed for the (3 × 1) structure, the Br–Pt bonding distance is nearly the same for the short-bridge (2.48 Å) and the long-bridge site (2.56 Å). The values are very close to the ideal covalent bond length of 2.50 Å. The buckling of the Br layer amounts to 0.25 Å, very close to the case of the (3 × 1) structure. The top-layer Pt atoms show a peculiar displacement pattern: The long-bridge Pt atoms are strongly outward shifted by 0.18 Å (compared to 0.25 Å for the (3 × 1) structure), whereas the horizontal distance from each other is increased by 0.2 Å. The short-bridge Pt atoms in turn are paired, reducing their mutual distance by 0.18 Å. The

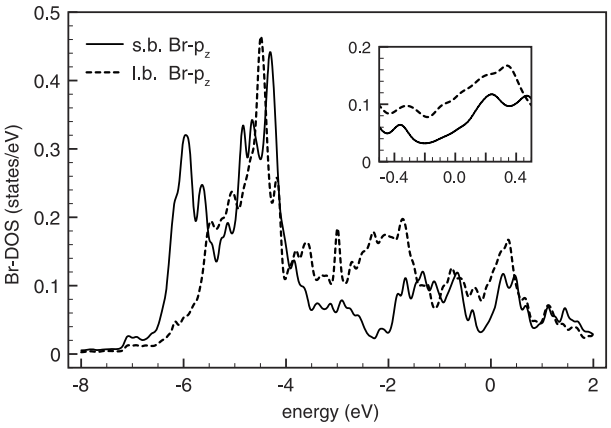


**Figure 6.** Comparison of the Br-p$_z$ like density-of-states (DOS) for short-bridge (s.b.) and long-bridge (l.b.) site Br atoms of the (4 × 1)-Br/Pt(110) structure.

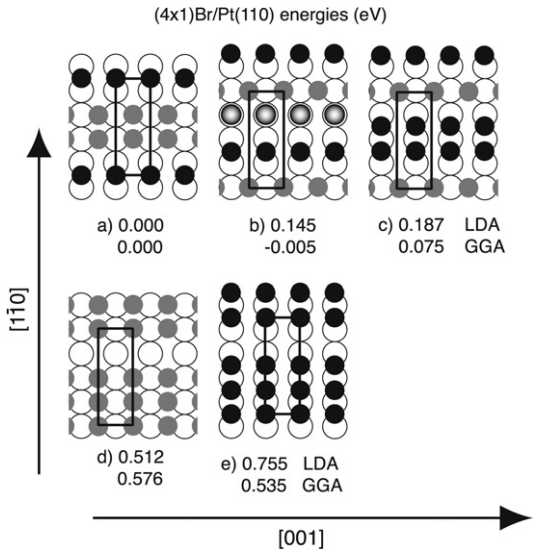


**Figure 7.** Relative adsorption energies for various Br arrangements with fourfold periodicity along the close-packed Pt rows. Empty circles denote the top-layer (1 × 1) Pt atoms and Br atoms are represented by filled black (short-bridge, s.b.), gradient filled (top), and gray (long-bridge, l.b.) circles. The configurations shown are starting positions, energies are given for Br atom positions fully relaxed in the [1$\bar{1}$0] direction, i.e. along the close-packed row direction.

most notable displacement in the second layer is an outward movement by 0.17 Å of the Pt atom beneath the two long-bridge sites so as to partially fill the gap caused by the anti-pairing of the latter.

In concluding the presentation of the IV-LEED results we remark that it was impossible to achieve reasonable Pendry $R$ factors with substitutional adsorption models.

Turning to the DFT calculations, the excellent agreement between experiment and simulated images employing the Tersoff–Hamann model has already been noted in figures 4(a) and (c). One might wonder why the difference in contrast between the short-bridge and long-bridge Br atom is not as large as one could anticipate from the different geometrical heights (short bridge > long bridge by 0.25 Å). The answer is evident from figure 6, where the density-of-states (DOS) is shown for both types of Br atoms. Actually only the Br-p$_z$ like DOS is displayed, which due to the protruding p$_z$ orbitals is largely responsible for the STM signal. Evidently, at experimental bias voltages the p$_z$ like DOS for the long-bridge Br atom is much higher than for the short-bridge one, thus partly compensating for the difference in geometrical height. A detailed comparison between DFT and LEED regarding the geometrical parameters for the (4 × 1)-Br/Pt(110) structure is given in table 1. There, the quality of the DFT calculations is assured by employing two different XC-potentials (GGA and LDA), as well as Pt substrate slabs of different thickness (9 and 11 layers).

Quite clearly, except for the Br height neither the type of XC potential nor the increased slab thickness changes the values of the calculated parameters by more than the error bars imposed by experiment, typically by less than 0.02 Å when increasing the slab thickness, and at most by 0.04 Å ($x_{13}$ and $x_{14}$) when switching from LDA to GGA. The Br height $d_{\mathrm{Br}}$ is reduced by 0.06 Å for LDA, which is in better agreement with the LEED data. Quite generally, the question of always favoring GGA over LDA has to be reconsidered for systems involving 5d elements such as Pt. LDA does a better job for the bulk properties of these systems, as shown recently in a comparative study [20], and yields a substrate bulk interlayer spacing close to experiment, with consequences for the adsorbed Br atoms due to the reduced lateral lattice constant as compared to GGA, as will be discussed below. The agreement between LEED and DFT slightly favors LDA over GGA, although the latter values are also mostly within the respective experimental error limits. Inspecting the LDA values more closely, one finds the largest deviation from experiment for the lateral repulsion of the long-bridge Br atoms ($x_{\mathrm{Br2}}$) and the pairing of the Pt atoms involved in the short-bridge Br–Pt bond ($x_{11}$, $x_{12}$) which is larger by as much as 0.05 Å in the LEED analysis. This trend is reversed for the Pt substrate buckling in the first and second layer ($z_{11}$, $z_{13}$ and $z_{21}$, $z_{22}$) where LEED finds a smaller buckling, which extends down to the third and even the fourth Pt layer in agreement with the calculations. Nevertheless, although small, these discrepancies between LEED and DFT raise the question of whether other structural models could be excluded. Guided by previous experience with the Br/Pt system, which concluded that a repulsive substrate mediated interaction between the Br atoms on the various adsorption sites is very important for the formation of Br surface structures, other models such as that shown in figure 7 might be possible candidates for a (4 × 1) Br/Pt surface structure. The energies given in figure 7 are the differences with respect to the LEED (DFT) structural model of figure 5 and table 1, with one short-bridge and two long-bridge sites occupied by Br atoms in the 4 × 1 cell. Minimizing the long-bridge repulsion by placing one Br atom on a top site just above a Pt atom in model (b) surprisingly leads to a lower energy for GGA. LDA, however, due to the smaller lateral substrate spacing tends to strengthen the two long-bridge Br–Pt bonds of model (a) while the repulsion is less efficiently reduced and thus yields a less stable structure for model (b). The gain in adsorption energy for short-bridge sites

over long-bridge sites is offset by the larger repulsion between the neighboring short-bridge Br atoms in model (c). This trend is more pronounced for LDA than for GGA, again due to the smaller in-plane lattice constant. Both LDA and GGA agree that models (d) and (e) which account for 'missing'-row structures are least stable due to the vastly increased repulsion between neighboring Br atoms.

Summarizing the DFT results we find a very good correspondence between the calculated and LEED determined structural parameters. DFT and LEED agree that the structure of model (a) is the most stable one. However, its overall stability is sensitive to the chosen (LDA versus GGA, with LDA very close to experiment) Pt substrate lattice constant, due to a delicate interplay between repulsive interactions and on-site adsorption energies for the various possibilities to occupy short-bridge and long-bridge sites in a $(4 \times 1)$ structure.

## 4. Discussion

The displacement pattern of the top-layer Pt atoms is to some extent similar to the one observed for the $(3 \times 1)$ structure: the long-bridge atoms are outward shifted. As there are two neighboring long-bridge sites involved, the buckling is consistent with a soft Rayleigh phonon of fourfold periodicity. A concomitant charge density modulation can be anticipated from the alternating pairing–anti-paring pattern along the close-packed Pt rows. Thus the structure seems compatible with a Peierls mechanism. In this model the Peierls distortion of the substrate is the primary effect. The outward buckling of the long-bridge Pt atoms and the associated charge accumulation renders the long-bridge sites more favorable and leads to a gradual switching from a short-bridge to long-bridge site population. The sequence of Br induced $(n \times 1)$ structures in this interpretation would then constitute another case of a tunable CDW as proposed for the Br/CO and the Br/NO co-adsorption systems [21, 22]. Further examination of such a model requires a precise mapping of the Fermi surface shifts occurring upon an increase of the Br coverage to 0.75 ML.

Alternatively, the substrate buckling could be attributed to short-range interactions with the Br atoms. Following this line of argument, the displacement pattern in the Pt top layer is explained by the tendency to maintain the optimum bond length to the Br atoms and simultaneously to minimize the buckling in the Br adatom layer. As a consequence, the Pt atoms forming the long-bridge adsorption site are pulled outwards. However, given the short-bridge site as the most favorable adsorption site for Br one should assume that a complementary $(4 \times 1)$ unit cell with two neighboring occupied short-bridge sites in the center and occupied long-bridge sites at the corners is the most favorable geometry. This is not confirmed by LEED and by the DFT calculations. A rationale for the switch to a majority of long-bridge sites is provided in terms of the large repulsive interaction of Br on neighboring short-bridge sites, which amounts to 1.21 eV [11] in the unrelaxed case. The repulsive interaction is considerably smaller for the occupation of neighboring long-bridge sites, namely only 0.8 eV. Thus the reduced repulsion compensates for the less favorable binding energy in the long-bridge site.

**Table 2.** Comparison of the structural parameters for the $(4 \times 1)$ structure found in the present study (figure 7(a)) and the 'inverted' $(4 \times 1)$ structure (figure 7(c)). Br1 refers to the short-bridge (s.b.) and Br2 to the long-bridge (l.b.) site.

| $(4 \times 1)$ s.b. + l.b. + l.b. (figure 7(a)) | | | | | | | |
|---|---|---|---|---|---|---|---|
| $d_{Br}$ | $\Delta d_{12}$ | $\Delta d_{23}$ | $\Delta d_{34}$ | $\Delta d_{45}$ | $z_{Br1}$ | $z_{Br2}$ | $x_{Br2}$ |
| 1.77 | −0.03 | 0.01 | 0.02 | −0.01 | 0.16 | −0.08 | −0.34 |
| $z_{11}$ | $z_{12}$ | $z_{13}$ | $z_{14}$ | $x_{11}$ | $x_{12}$ | $x_{13}$ | $x_{14}$ |
| −0.12 | −0.12 | 0.12 | 0.12 | 0.04 | −0.04 | −0.08 | 0.08 |
| $z_{21}$ | $z_{22}$ | $z_{23}$ | $z_{24}$ | $x_{21}$ | $x_{22}$ | $x_{23}$ | $x_{24}$ |
| −0.10 | −0.01 | 0.12 | −0.01 | 0.00 | 0.03 | 0.00 | −0.03 |
| $z_{31}$ | $z_{32}$ | $z_{33}$ | $z_{34}$ | $z_{41}$ | $z_{42}$ | $z_{43}$ | $z_{44}$ |
| −0.04 | −0.04 | 0.04 | 0.04 | −0.05 | 0.00 | 0.04 | 0.00 |
| $(4 \times 1)$ l.b. + s.b. + s.b. (figure 7(c)) | | | | | | | |
| $d_{Br}$ | $\Delta d_{12}$ | $\Delta d_{23}$ | $\Delta d_{34}$ | $\Delta d_{45}$ | $z_{Br1}$ | $z_{Br2}$ | $x_{Br1}$ |
| 1.91 | −0.04 | 0.02 | 0.01 | 0.00 | 0.12 | −0.24 | −0.36 |
| $z_{11}$ | $z_{12}$ | $z_{13}$ | $z_{14}$ | $x_{11}$ | $x_{12}$ | $x_{13}$ | $x_{14}$ |
| 0.07 | −0.13 | 0.20 | −0.13 | 0.00 | −0.04 | 0.00 | 0.04 |
| $z_{21}$ | $z_{22}$ | $z_{23}$ | $z_{24}$ | $x_{21}$ | $x_{22}$ | $x_{23}$ | $x_{24}$ |
| −0.03 | 0.03 | 0.03 | −0.03 | −0.02 | 0.03 | −0.03 | 0.02 |
| $z_{31}$ | $z_{32}$ | $z_{33}$ | $z_{34}$ | $z_{41}$ | $z_{42}$ | $z_{43}$ | $z_{44}$ |
| −0.03 | −0.02 | 0.07 | −0.02 | −0.03 | 0.03 | 0.03 | −0.03 |

The repulsion is further reduced by the displacement in $[1\bar{1}0]$ direction of the long-bridge Br atoms, which increases their distance by 0.76 Å.

This local-interaction model poses essentially two problems: first, an *ad hoc* assumption has to be introduced concerning the tendency to minimize the buckling of the Br ad-layer. As there is no direct Br–Br interaction, it is unclear, why it should be more favorable to pull out the long-bridge Pt atoms rather than to move in the long-bridge Br atoms somewhat further. Secondly, one has to provide a rationale for the strongly differing repulsion of Br in neighboring long-bridge and short-bridge sites, respectively. Taking into account the identical distances and the very similar bonding character this has to be attributed to differences in the substrate mediated interaction, apparently the repulsive Br–Br interaction is mediated much more efficiently by electronic states localized on the close-packed rows than by those in the troughs. This supports angle-resolved photoemission data indicating the existence of quasi-1D electronic surface resonances localized on the close-packed Pt rows [2, 3].

Looking at the problem from a different perspective one could also focus on the elastic, rather than the electronic, properties of the substrate. For this purpose it is interesting to compare the lattice distortions arising in the $(4 \times 1)$ structure identified here (figure 7(a)) and the competing, 'inverted' structure (figure 7(c)) with a majority of short-bridge sites. The corresponding structural data as obtained from an 11-layer LDA calculation are given for both unit cells in table 2. Figure 8 provides a qualitative sketch of the substrate buckling in the two cases. For the actually observed structure the buckling of the top Pt layer can be described by a sinusoidal modulation of the $z$ coordinate with a single wavevector $k_{\text{buckling}} = 1/4G$, where $G$ is a reciprocal lattice vector. This is not the case for the 'inverted' structure (figure 7(c)): here sinusoidal modulations with at least two different wavevectors ($1/4G$ and $1/2G$) have to be superposed in order to describe

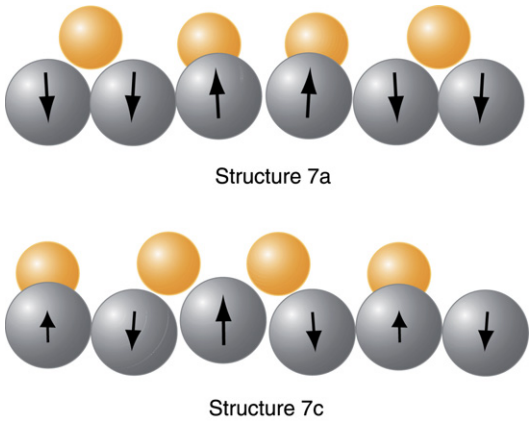


**Figure 8.** Buckling pattern for the observed (4 × 1) structure (figure 7(a)) with one short-bridge and two long-bridge sites per unit cell and the 'inverted' (4 × 1) structure (figure 7(c)) with one long-bridge and two short-bridge sites per unit cell.

the displacement pattern. Intuitively one would expect that the simpler displacement pattern is also energetically more favorable.

Of course elastic and electronic properties are intertwined. Lattice distortions (respectively frozen phonons) and charge density modulations are inseparable in the present system. In both the Peierls and the local-interaction model quasi-1D surface resonances play an essential role in shaping the phase diagram. The first model is based on a Fermi surface instability. This corresponds to an interaction localized in $k$ space and hence long-ranged in real space. The second model emphasizes short-range interactions in real space which in turn implies participation of several electronic states with an extended range of $k$ vectors. In other words, here the interaction is delocalized in reciprocal space. The preference for a buckling pattern with a single wavevector $k_{\text{buckling}} = 1/4G$ seems to support the non-local Peierls model. In this case it should be possible to predict the evolution of the adsorbate phases as a function of coverage and temperature from monitoring changes in the Fermi surface by angle-resolved photoemission. While the photoemission data collected so far seem to hint at the first scenario [23, 24], further work is necessary in order to see whether the second model can be ruled out. In a wider perspective, the validity of the Peierls model would substantiate the idea of tuning the phase diagram by appropriate manipulation of surface states or surface resonances [25].

In summary, the convergence of IV-LEED data and first-principles calculations obtained in the present study once again demonstrates the high reliability of structure determination using a combination of both. Only on the basis of such a precise structure analysis will it be possible to obtain a detailed understanding of the interplay between surface electronic structure and adsorbate phase diagrams. In the present case the analysis tends to support the Peierls mechanism. It clearly demonstrates the important role of quasi-1D surface resonances in shaping the peculiar phase diagram and the anomalous phase transitions ('reverse' order–disorder transition [7]) in the Br/Pt(110) system. Further investigation of these phases by angle-resolved photoemission should help us to understand the energetics of this interesting, strongly anisotropic system.

## Acknowledgments

Financial support by the Austrian Science Fund (FWF) and by the West Austrian Initiative for Nano-Networking (WINN) is gratefully acknowledged.

## References

[1] Swamy K, Menzel A, Beer R and Bertel E 2001 *Phys. Rev.* B **86** 1299
[2] Menzel A, Zhang Zh, Minca M, Loerting T, Deisl C and Bertel E 2005 *New J. Phys.* **7** 102
[3] Minca M, Penner S, Dona E, Menzel A, Bertel E, Brouet V and Redinger J 2007 *New J. Phys.* **9** 386
[4] Zhang Zh, Minca M, Deisl C, Loerting T, Menzel A, Bertel E, Zucca R and Redinger J 2004 *Phys. Rev.* B **70** 121401(R)
[5] Minca M, Penner S, Loerting T, Menzel A, Bertel E, Zucca R and Redinger J 2007 *Top. Catal.* **46** 161
[6] Blum V, Hammer L, Heinz K, Franchini C, Redinger J, Swamy K, Deisl C and Bertel E 2002 *Phys. Rev.* B **65** 165408
[7] Dona E, Loerting T, Penner S, Minca M, Menzel A, Bertel E, Schoiswohl J, Berkebile St, Netzer F, Zucca R and Redinger J 2007 *Phys. Rev. Lett.* **98** 186101
[8] Dona E, Amann P, Cordin M, Menzel A and Bertel E 2008 *Appl. Surf. Sci.* **254** 4230
[9] Grüner G 1994 *Density Waves in Solids* (Reading, MA: Addison-Wesley)
[10] Rice T M and Scott G K 1975 *Phys. Rev. Lett.* **35** 120
[11] Deisl C, Swamy K, Memmel N, Bertel E, Franchini C, Schneider G, Redinger J, Walter S, Hammer L and Heinz K 2004 *Phys. Rev.* B **69** 195405
[12] Hanesch P and Bertel E 1997 *Phys. Rev. Lett.* **79** 1523
[13] Blum V and Heinz K 2001 *Comput. Phys. Commun.* **134** 392
[14] Kresse G and Furthmüller J 1996 *Phys. Rev.* B **54** 11169
VASP group *Vienna Ab-Initio Simulation Package* http://cms.mpi.univie.ac.at/vasp/
[15] Blöchl P E 1994 *Phys. Rev.* B **50** 17953
[16] Kresse G and Joubert D 1999 *Phys. Rev.* B **59** 1758
[17] Wang Y and Perdew J P 1991 *Phys. Rev.* B **44** 13298
[18] Perdew J P and Zunger A 1981 *Phys. Rev.* B **23** 5048
Ceperley D M and Alder B J 1980 *Phys. Rev. Lett.* **45** 566
[19] Tersoff J and Hamann D R 1985 *Phys. Rev.* B **31** 805
[20] Tran F, Laskowski R, Blaha P and Schwarz K 2007 *Phys. Rev.* B **75** 115131
[21] Swamy K, Deisl C, Menzel A, Beer R, Penner S and Bertel E 2002 *Phys. Rev.* B **65** 121404
[22] Deisl C, Swamy K, Beer R, Menzel A and Bertel E 2002 *J. Phys.: Condens. Matter* **14** 4199
[23] Swamy K, Deisl C, Menzel A, Beer R, Penner S and Bertel E 2002 *Phys. Rev.* B **65** 121404
[24] Deisl C, Swamy K, Beer R, Menzel A and Bertel E 2002 *J. Phys.: Condens. Matter* **14** 4199
[25] Bertel E and Doná E 2007 *J. Phys.: Condens. Matter* **19** 355006